Title: Progressive cracking of masonry arch bridges

Authors:
Niamh Gibbons**,** BAI MA MSc PhD
Research Associate**,** Department of Engineering, University of Cambridge**,** United Kingdom

Paul J. Fanning, BE PhD CEng FIEI
Senior Lecturer, School of Civil, Structural & Environmental Engineering, University College Dublin, Ireland

Abstract:
Numerous methods are available for the assessment of masonry arch bridges at the ultimate limit state, however there is a lack of suitable methods for assessing behaviour at service levels of loading. To address this, nonlinear three dimensional finite element models which consider constitutive material models enabling progressive cracking and failure of the complete structural system were used to investigate the development of damage for three masonry arch bridges at both service levels and at the ultimate capacity. All of the elements contributing to the strength of structure were represented in the models including the arch barrel, spandrel, abutments, fill and surrounding soil. This allowed for consideration of the longitudinal and transverse capacities, the stiffening effects of the spandrel walls, the restraint and load distribution provided by the fill, the frictional behaviour between the masonry and fill, movement at the abutments and multiple causes of failure. While complex nonlinear finite element models are able to identify the ultimate load capacity there are alternate simpler approaches available for this, and it is the investigation of damage and crack propagation at service level loads where their use is of greatest benefit.

Notation:

c cohesion
f_1 ultimate compressive strength for a state of biaxial compression superimposed on the ambient hydrostatic stress state
f_2 ultimate compressive strength for a state of uniaxial compression superimposed on the ambient hydrostatic stress state
f_c ultimate uniaxial compressive strength
f_{cb} ultimate biaxial compressive strength

f_t ultimate uniaxial tensile strength

E Young's modulus

β_t shear transfer coefficient for an open crack

β_c shear transfer coefficient for a closed crack

μ coefficient of friction

ν Poisson's ratio

ρ density

σ_h hydrostatic stress state

σ_h^a ambient hydrostatic stress state

σ_{xp}, σ_{yp}, σ_{zp} principal stresses in principal directions

ϕ angle of internal friction

ϕ_f angle of dilatancy

1 Introduction

Masonry arch bridges have a complex relationship with damage. Prior to failure, extensive damage occurs via the formation of multiple hinges or other damage patterns, and this presents challenges for both the analysis of the failure capacity and the question of how much and what damage is acceptable under operating loads. The level of loading at which damage begins to occur is also difficult to quantify, as is the large reserve in strength beyond the first signs of damage. This can result in uncertainty over the significance of existing damage or in overconfidence in assessed capacities which may be quickly undermined by the introduction of new loading regimes.

Masonry arches are arguably the most durable and sustainable bridge type and there is a high level of confidence in their capacity which is reflected in current assessment practices which only consider the ultimate capacity state (Highways Agency, 1997; Network Rail, 2006), ignoring the preceding damage and associated change in stiffness of the structure. There are currently no serviceability limits specified for the assessment masonry arch bridges. Correspondingly, the analysis methods most commonly employed for the assessment of masonry arches, such as limit analysis methods (Kooharian, 1952; Heyman, 1982; Delbecq, 1982; Crisfield and Packham, 1987; Harvey, 1988; Gilbert and Melbourne, 1994; Hughes et al., 2002) and empirically based methods (Highways Agency, 1997; Network Rail, 2006), identify only an ultimate capacity failure load. This paper presents nonlinear three

dimensional finite element (FE) models which not only allow for more realistic representation of the failure mechanisms but also consider progressive damage in the structure allowing for interrogation of existing damage and investigation of behaviour at service level loads for masonry arch bridges, shifting focus away from the ultimate capacity and towards the more problematic area of new and existing damage for bridges assessed as having adequate capacity based on ultimate load levels.

2 Background

Masonry arch bridges are generally assessed with two dimensional methods which offer minimal computational expense but which necessitate numerous simplifying assumptions and limit the type of failure mechanisms that can be considered. The assumptions made for two dimensional assessments vary from method to method, but their obvious drawback is that they cannot assess the transverse capacity of the arch. This has further implications for assumptions regarding load distribution. For example, the transverse load distribution model in BD 21/01 (Highways Agency, 2001) is based on the depth of fill plus an additional further width in order to account for the transverse capacity of the barrel. However there is no assessment of the transverse capacity of the arch to ensure that this assumption is valid. Masonry arch bridges frequently exhibit longitudinal cracks owing to transverse bending in the barrel and in the presence of existing longitudinal cracks the transverse load distribution is limited by the resulting barrel width. However this focuses on the effects that the longitudinal cracks have on the longitudinal capacity of the arch in spite of their presence being a clear indication of a lack of transverse capacity which, at best, results in assessment of the longitudinal capacity under an increased load, rather than assessing for transverse failure. Furthermore, it fails to account in any manner for longitudinal cracking which may occur as the loading approaches the ultimate capacity for which the structure is being assessed, resulting in adequate transverse capacity being assumed when approaching the ultimate capacity based on behaviour under lower, generally unknown, working loads.

Another characteristic of two dimensional approaches is the exclusion of the spandrel walls which serve to retain the fill material and stiffen the arch barrel at either edge, although there are a number of exceptions: Melbourne et al. (1997) incorporated the spandrel walls into a rigid block limit analysis as large blocks arguing that the structures considered were sufficiently narrow and the experimentally observed three dimensional effects limited enough to do so, and Cavicchi and Gambarotta (2007) introduced a limiting transverse compressive

stress to the fill in order to account for the limits to the constraint provided by the spandrel walls. Nevertheless the differential stiffness across the width of the barrel caused by the presence of the spandrel walls cannot be accounted for fully with a two dimensional analysis. While the beneficial effects of the spandrel walls on the ultimate load capacity has been demonstrated (Royles and Hendry, 1991; Melbourne et al., 1997) it has also been recommended that the integrity of the spandrel walls with the arch barrel should not be relied upon for the purposes of ultimate capacity assessment (Page, 1993; Fanning et al., 2005). However it is possible to incorporate damage at the spandrel arch interface into a nonlinear three dimensional analysis, as is demonstrated in this paper, and the restraint provided by the spandrel walls which influences the magnitude of deflections, the crack patterns and the ensuing failure mechanisms. Therefore, consideration of the spandrel walls as part of a three dimensional analysis provides a better representation of the structural response, allowing for interpretation of existing damage and a more accurate prediction of the effects of increased loading. Furthermore, the spandrel walls may also be subject to failure themselves and a three dimensional analysis allows for consideration of this failure mechanism.

Full width three dimensional approaches (Tao, 2003; Fanning and Boothby, 2001; Rafiee et al., 2008; Robinson et al., 2010; Milani and Lourenco, 2012; Behnamfar and Afshari, 2013) negate the need for many of the simplifying assumptions required for two dimensional approaches regarding load distribution, transverse behaviour and support conditions. They also allow for the greatest level of flexibility in representing the structure and investigating the contribution of different elements to the response. Despite the significance of both the three dimensional response and the nonlinear behaviour of masonry arch bridges, the use of these methods has to date been limited in practice. However, if conditions other than ultimate failure are to be considered three dimensional nonlinear analysis offers the greatest potential.

Experimental data for the purposes of validating a three dimensional model at the ultimate capacity level are to date limited. Page (1993) provides a comprehensive overview of load tests carried out both on full scale in-situ masonry arch bridges and on laboratory models with the accompanying comment that the “completeness of the data describing the bridges and the tests varies considerably” making the suitability of the test data for the validation of analysis challenging, although this reflects the conditions typically encountered with the assessment of real structures. What presents a greater challenge for the validation of a three dimensional analysis is that the majority of both full scale in-situ tests and laboratory tests

loaded to failure have been constructed so as to replicate two dimensional conditions through the loading arrangements and/or the removal of different components of the structure. For example Davey (1953) summarized the results of tests on 22 bridges carried out by the Building Research Station, three of which were tested to destruction. Prior to testing, the parapet walls were removed from one of the structures and the parapet walls, spandrel walls and fill were removed from another. The Transport and Road Research Laboratory (TRRL) carried out a series of tests to collapse on eight decommissioned structures (Hendry et al., 1985; Hendry et al., 1986; Page, 1987; Page, 1988; Page, 1989) and two full scale laboratory models (Harvey et al., 1989; Melbourne and Walker, 1990). These bridges were tested to failure effectively under line loads applied across the width of the bridge and in the case of Prestwood Bridge (Page, 1987) with the parapet walls removed. Data for laboratory tests are more detailed and are available with varying combinations of arch, fill and spandrel walls both at large scale (Pippard and Ashby, 1939; Towler, 1981; Hodgson, 1996; Melbourne and Gilbert, 1995; Melbourne et al., 1997; Ng, 1999; Tao, 2003; Robinson et al., 2010; Callaway et al., 2012) and at model scale (Royles and Hendry, 1991; Fairfield and Ponniah, 1994; Hughes et al., 1998; Ponniah and Prentice, 1998) but again with the loading applied across the full width of the arch to replicate two dimensional conditions. Wang (2004) deviated from this type of loading arrangement, carrying out large scale tests to failure using patch loads applied directly to the arch barrel with no fill or spandrel walls and reported that all of the arches demonstrated a three dimensional transverse response. In-situ service load tests on fully intact structures under passing vehicles provide the most realistic conditions, both in terms of the loading and condition of the structure. With all of the elements contributing to the structural response in place and in the absence of constraints designed to replicate two dimensional conditions, service load tests have clearly exhibited the effects of transverse bending in the arch barrel (Page, 1995; Boothby et al., 1998; Fanning and Boothby, 2001; Fanning et al., 2005; Sustainable Bridges, 2007). Testing under service loads provides suitable data for comparison with a three dimensional analysis but has the drawback however of usually only being applicable in the linear range of behaviour. In the absence of suitable load tests to destruction a combination of the following have been used to validate the three dimensional models presented in this paper:

- service level load tests,
- high level load tests,
- correlation with existing damage patterns.

3 Description of bridges

Three dimensional nonlinear finite element analyses were carried out for three masonry arch bridges. The three bridges are all single span structures of stone construction. While varying in span, construction details and materials, these bridges can all be considered common masonry arch bridge types as encountered in Ireland displaying characteristics typical for their purposes. The bridges consist of a canal bridge, a railway overbridge and a rural road bridge crossing a small river. The dimensions for each of the bridges are summarized in Table 1.

Griffith Bridge, shown in Figure 1, is an over bridge for the Grand Canal in Dublin carrying road traffic. Constructed in 1791, it forms part of set of elliptical or three-centred profile arches which were constructed in series and named after various directors of the Grand Canal Company. Griffith Bridge is 9.45 m in span with a ring thickness of 0.446 m. The arch barrel is of ashlar limestone construction with granite fascia stones and mortar joints approximately 5 mm wide. The spandrel walls are of limestone construction with 10 mm joints and granite capping stones. The depth of fill at the crown is 0.126 m.

Greenfield Bridge, Figure 2, was constructed as part of the Cork and Macroom Direct Railway line opened in 1866. It served as an overbridge for road traffic until it was put offline by the construction of the Ballincollig Bypass which was completed in 2004. The arch has a segmental profile and is 4.52 m in span. The arch barrel, spandrel, parapet and wing walls are constructed from squared limestone units with approximately 10 mm wide mortar joints. The arch ring is 0.465 m thick with 0.126 m of fill at the crown.

O'Connell's Bridge, Figure 3, is a 10.36 m span bridge crossing the Gleensk River on the Iveragh Peninsula, County Kerry. It is constructed from Old Red Sandstone, a siliceous or non-calcareous sandstone from the Devonian Period. The masonry is of random rubble construction with large irregular mortar joints. The depth of the fascia stones of the arch vary, however an average value of 0.610 m has been taken for the ring thickness. The depth of fill at the crown is 0.100 m and the width of the bridge is 6.77 m. Prior to recent repairs O'Connell's Bridge exhibited significant longitudinal cracking of the arch barrel, Figure 4.

4 Finite element models

4.1 Material models and material properties

The bridges were modelled using ANSYS v13, a general purpose finite element software package. The masonry units and mortar were treated as a single continuous material with reduced values assigned for stiffness and strength compared with that of the stone itself. The fill, backing and road surfacing were also treated as a single material. The materials properties that were assumed for the masonry and the fill material for each of the bridges are summarised in Table 2.

Eight noded isoparametric SOLID65 elements with 2 x 2 x 2 Gaussian integration points which allow for nonlinear material behaviour in the form of cracking, crushing and plastic deformation were used to model both the masonry and the fill material.

The masonry was assumed to behave elastic perfectly plastic in compression and elastic perfectly brittle in tension. A smeared crack concrete material model based on the Willam and Warnke failure criterion (Willam and Warnke, 1975; ANSYS Inc., 2010) to predict the failure of brittle materials was used. The material is initially assumed to be isotropic and if the principal stresses exceed the specified tensile capacity at one of the integration points a plane of weakness, or a smeared band of cracks, is introduced orthogonal to the principal stresses; reducing the stresses in this region and redistributing them locally. Where cracking has occurred in the model, rather than reducing the stiffness to zero, a very small stiffness value of $1x10^{-6}$ is assigned in order to provide numerical stability. Following the formation of the first crack, the material model is capable of forming a second and third crack in orthogonal directions for each integration point. This approach assumes a homogeneous masonry-mortar continuum with the crack locations dictated by the principal stresses. In reality, the exact location and orientation of the cracks will be determined by planes of weakness occurring in a composite material that is heterogeneous at multiple scales. Planes of weakness will typically occur along the mortar joints, but may also occur in the masonry units themselves where very stiff cementitious mortar has been used with weaker stone or brick. Stone masonry units may also be highly anisotropic, exhibiting large variations in strength with orientation, as for example with sedimentary rock types. The size and composition of units within a given bridge can also be highly variable. In addition, a wide variety of mortars can be found on a single bridge, commonly consisting of a combination of older lime mortars and newer cementitious repointing. Micromodelling approaches can be

employed to address a number of these issues, however it can be very challenging to ascertain the existing heterogeneity of the materials and a number of simplifying assumptions are still required in order to produce a reasonable model and achieve numerical efficiency. This often includes representing the masonry and mortar joints in a regular arrangement and therefore still presents limitations in terms of identifying the exact location of cracks.

The parameters that define the failure surface for the smeared crack concrete material model are the ultimate uniaxial compressive strength, f_c, the ultimate uniaxial tensile strength, f_t, the ultimate biaxial compressive strength, f_{cb}, the ambient hydrostatic stress state, σ_h^a, the ultimate compressive strength for a state of biaxial compression superimposed on the ambient hydrostatic stress state, f_1, and the ultimate compressive strength for a state of uniaxial compression superimposed on the ambient hydrostatic stress state, f_2. However, provided the hydrostatic stress state, σ_h, defined as the average of the principal stresses as per Equation 1, meets the condition set out in Equation 2, the failure surface can be defined using only two parameters, f_t and f_c, and values for the parameters f_{cb}, f_1, and f_2 can be assumed as per Equation 3 – Equation 5 (Willam and Warnke, 1975; ANSYS Inc., 2010).

Equation 1 $$|\sigma_h| \leq \sqrt{3}\, f_c$$

Equation 2 $$\sigma_h = 1/3\, (\sigma_{xp} + \sigma_{yp} + \sigma_{zp})$$

Equation 3 $$f_{cb} = 1.2\, f_c$$

Equation 4 $$f_1 = 1.45\, f_c$$

Equation 5 $$f_2 = 1.725\, f_c$$

The ultimate uniaxial compressive strength of the masonry, f_c, was determined based on the geological classification of the stone and the quality of masonry work as per BD 21/01 (Highways Agency, 2001) and Hendry (1990), and in the case of Greenfield Bridge on compressive strength tests which were carried out on three stone samples taken from the spandrel walls (Fanning and Boothby, 2005). A low hydrostatic stress state was assumed for the masonry and therefore f_{cb}, f_1, and f_2 were determined as per Equation 3 – Equation 5. The values for the Young's modulus of the masonry were based on recommendations set out in Boothby and Fanning (2004), and in the case of Greenfield Bridge from strain measurements taken during the compressive tests (Fanning and Boothby, 2005).

Shear transfer coefficients for open and closed cracks, β_t and β_c respectively, may also specified in the concrete material model, altering the stress strain matrix when cracking occurs in order to account for shear transfer across the cracks. A value of 0.0 represents no shear transfer, i.e. a smooth crack, and a value of 1.0 represents full shear transfer. The inclusion of nominal values of 0.01 for the shear transfer coefficients were included in the material model for the purposes of numerical stability.

A limited tensile strength, f_t, equal to 5% of the compressive strength was assigned to the masonry. Tensile capacity in the analysis of masonry arches is a long contested issue. Historically the analysis of masonry arches assumed a no tension criterion: the middle third rule (Young, 1817; Navier, 1826; Rankine, 1858) ensured that the entire section was kept in compression and prevented any tension from occurring and Castigliano's method (1879) assumed that the arch had no tensile capacity resulting in thinning of the arch section where tension occurred. Pippard (1948) broke from the no tension criterion arguing that even a weak lime mortar would be able to carry some tension and allowed for values up to 0.7 MPa based on experimental results reported in Pippard and Ashby (1939). However Heyman (1966) argued that the joints would have no tensile capacity in a dry stone arch or in the presence of weak mortars and would only transmit tension through interlocking of the stones if the arch was of random rubble construction, as opposed to cut stone voussoirs, and set out zero tensile capacity as the first assumption of limit design for arches. While the exclusion of any tensile capacity is often adopted on the basis of being conservative, nonlinear finite element approaches have shown that ultimate capacity predictions are highly sensitive to it as a parameter and that its inclusion is necessary for correlation with experimental results (Towler, 1981; Crisfield, 1985; Yang, 1991; Ng, 1999; Fanning et al., 2005; Robinson et al., 2010), with the inclusion of even nominal values providing greater numerical stability for nonlinear solutions.

The fill material was treated as elastic-perfectly plastic and a Drucker-Prager yield criterion was used (Drucker and Prager, 1952; ANSYS Inc., 2010). This uses an outer cone approximation to fit a smooth yield surface around the Mohr-Coulomb surface. The parameters used for the Drucker-Prager material model are cohesion, c, the angle of internal friction, ϕ, and the dilantancy angle, ϕ_f. Either an associative flow rule, with the dilantancy angle equal to the angle of internal friction, or a nonassociative flow rule, with the dilantancy angle less than the angle of internal friction, can be used to control the increase in volume due

to yielding. The associative flow rule was used for the models presented in this paper. For all of the bridges the fill material was not precisely known, however the fill was assumed to be highly compacted having been subjected to over 100 years of loading and high stiffness values were required in order to capture the limited abutment responses measured during the service load testing for Griffith Bridge and Greenfield Bridge. The fill was assumed to have a Young's modulus of 0.5 GPa, Poisson's ratio of 0.23, a cohesion value of 1000 Pa and both the angle of internal friction and the dilantancy angle equal to 44 degrees.

Eight noded surface-to-surface contact elements were used at the interface between the masonry and fill with an isotropic Coulomb friction model. This allows the material to 'stick' and then 'slide' when the shear stress exceeds the limiting frictional stress, allowing the fill to move along the surface of the masonry. The limiting frictional stress is determined by the product of the frictional coefficient, μ, and the normal contact pressure. For the bridges modelled in this paper a frictional coefficient of 0.2 was applied.

4.2 Finite element mesh and boundary conditions

For Griffith Bridge and O'Connell's Bridge both the bridge geometry and the loading were symmetric about the centreline and half width models were used. For Greenfield Bridge a full width model was used as the geometry of the parapet walls differed on either side and for the high level load tests the loading was asymmetric. For all of the bridges the fill was modelled 6 m beyond the extent of the spandrel walls in order to ensure that the boundary conditions applied at the extremities of the fill did not interfere with the response at the abutments. The fill and the masonry were also extended 1 m below the springing point of the arch. Coarser meshing was used for the extended sections of fill and a more refined mesh was used along the line of the load path. The finite element mesh for Griffith Bridge is shown in Figure 7.

Compression only support was applied to the bottom faces of the fill and the masonry. The base of the 1 m section of masonry below the arch barrel was restrained against horizontal movement in the longitudinal direction. Compression only support was also applied to the vertical faces of the fill at either end of the model. The vertical face of the fill in line with spandrel wall and the section of masonry extended 1 m below the springing point were restrained in the normal direction against outward movement. Rather than modelling the wing

walls for Griffith Bridge and Greenfield Bridge as solid elements, the spandrel walls were restrained in the normal direction against outward movement at these locations.

5 Validation of finite element models

The finite element models were validated against a combination of service level load tests, high level load tests and existing damage patterns. The model for Griffith Bridge was validated against deflection responses at service load level. The model for Greenfield Bridge was validated against deflection responses at both service load levels and high load levels. The experimental testing programmes for Griffith Bridge and Greenfield Bridge are summarized below, further details of which can be found in Fanning and Boothby (2001) and Fanning et al. (2005). The model for O'Connell's Bridge was validated against existing damage patterns in the arch barrel. Further details of the model validation can be found in Gibbons (2014).

5.1 Load testing

For the service load testing, multiple passes of loaded construction vehicles at speeds less than 5 km/hr were made. Griffith Bridge was tested with a gross vehicle weight of 31.6 tonnes, consisting of a 1.7 m spaced double axle bogie at the front and a 1.42 m spaced double axle bogie at the rear, carrying approximately 10.5 tonnes and 21.1 tonnes respectively, with the front and rear bogies at a 5.56 m spacing. Greenfield Bridge was tested with a Volvo A25D articulated dumper with a gross vehicle weight of 45.5 tonnes, consisting of a single axle at the front and 1.67 m spaced double axle bogie at the rear, carrying approximately 14.1 tonnes and 31.4 tonnes respectively. The axle weights are summarized in Table 3. The bridges were instrumented with linear variable differential transformers (LVDTs) with a resolution of approximately 1 μm at a normal to the intrados of the arch and mounted on independent frames. Response measurements were taken at the crown, abutments and haunches at the LVDT locations shown in Figure 5 and Figure 6.

For Greenfield Bridge high level load tests were also carried out. Patch loads were applied by means of hydraulic jacks mounted against a steel reaction frame. The loads were applied and released incrementally in a series of steps from 15 tonnes up to 60 tonnes over two 0.3 x 0.6 m patches as shown in Figure 6. This was followed by loading over one patch up to 80

tonnes. For the 80 tonne load test, the loading was applied to the patch nearest the spandrel wall.

5.2 Service load test simulations

For Griffith Bridge and Greenfield Bridge a multi-step static analysis was used to simulate the slow moving vehicle loads applied during the on-site experimental testing programmes. In the first load step of each analysis, acceleration due to gravity was applied to the model. The inclusion of a self-weight load step is required in order to generate the in-situ stresses allowing for compressive load transfer in the arch and to account for deflections due to self-weight. In subsequent load steps static point loads were applied directly to the nodes of the fill material, as shown in Figure 7, moving across the bridge in 1 m increments.

5.2.1 Griffith Bridge

For Griffith Bridge, the experimental deflection responses at the crown centre for five passes of the loaded vehicle are plotted against the distance of the front axle from the crown in Figure 8. The peaks in response corresponding to the passing of the front and rear bogies are clearly distinguishable in the deflection response. The results of the service load simulation are plotted against the measured experimental data and show very good correlation both in magnitude and in capturing the peaks in deflection due to the passing of the front and rear axles. The maximum deflection at the crown centre is within 0.01 mm of the experimental results.

The contact pressures from the service load simulations at the interface between the masonry and the fill are shown in Figure 9 for the front of the vehicle located above the abutment, the haunch and the crown. At the abutments the load distribution through the fill material provided sufficient distribution to give loading conditions similar to two dimensional loading, adding compressive stress evenly across the base of the arch and pushing the barrel forwards in the longitudinal direction. However as the vehicle approaches the crown, the load distribution decreases leading to transverse bending in the barrel, illustrating the importance of considering the three dimensional transverse response where loads imparted to the barrel may be concentrated, typically at and near to the crown.

5.2.2 Greenfield Bridge

The experimental deflection responses for a passing vehicle load at three locations along the line of the crown of Greenfield Bridge are shown in Figure 10. Again, the peaks corresponding to the front and rear axles are clearly observable with a reduction in magnitude towards the edge of the structure demonstrating the three dimensional response of the arch barrel. Comparison of the initial service load simulation with the experimental results indicated that the model was overly stiff at the edge, suggesting damage at the spandrel arch interface. In order to test this hypothesis, damage was introduced to the finite element model using additional loading and unloading loadsteps prior to the moving vehicle load. The resulting deflections from the pre-damaged finite element model provided a more consistent correlation and are plotted against the measured experimental data in Figure 10.

5.3 High level load test simulations

The high level load tests carried out on Greenfield Bridge were applied as a series of load steps, applied and released incrementally from 15 tonnes to 60 tonnes over two patches, as shown in Figure 6, followed by loading over one patch to 80 tonnes in a single load step. Following an initial gravity step, a multi-step analysis was used to simulate the load tests as follows: loading to 60 tonnes and unloading over two patches; reloading to 60 tonnes and unloading over two patches; and loading to 80 tonnes over a single patch. The load deflection response under one of the patch loading areas at LVDT 2 is shown in Figure 11. As the 80 tonne load is not applied over same area as the 60 tonne load, it should be noted that the load deflection response for the 80 tonne load does not follow the same path as the 60 tonne load deflection response.

Good correlation with the experimental data was found following the initial 60 tonne load cycle. Following the damage incurred during the first load cycle, the second 60 tonne load cycle behaves in a linear manner, indicating existing damage in the structure prior to the high level experimental loading.

5.4 Simulation of existing damage

While no experimental load testing was carried out on O’Connell’s Bridge the in-situ structure exhibited damage in the form of a large longitudinal crack as shown in Figure 4. To

investigate the possible cause of the crack a double axle load was applied along the centreline above the haunch in 1 tonne increments. The first crack that formed in the arch barrel was longitudinal in direction, due to transverse bending of the arch, and occurred in line with the wheels of the double axle bogie at 20 tonnes, as shown in Figure 12, indicating that the existing crack is attributable to loading of the bridge under service level loads.

6 Legal load limit and ultimate capacity predictions

6.1 Loading

Current guidance for Ireland and the UK for the assessment of masonry arch bridges (Highways Agency, 1997; Highways Agency, 2001; National Roads Authority 2009) specifies the use of axle loads, rather than vehicle configurations or a uniformly distributed load with a knife edge load as is used for the assessment of other highway structures. Therefore in assessing the behaviour of the bridges at the legal load limit and up to the ultimate capacity, the validated finite element models were loaded with a double axle bogie with a 1.8 m axle spacing, with the wheel loads applied over 0.300 m x 0.300 m area. To carry out a full assessment other axle configurations would also need to be considered. As per Highways Agency (2001), load factors of 1.9 were applied to each of the axles and a further impact factor of 1.8 was applied to one of the axles. For Greenfield Bridge the vertical elevation of the road surface had a humped profile and so additional axle lift-off factors of 1.28 and 0.5 were also applied. No factor was applied to the dead load as this has a relieving effect for arches. The load factors are summarized in Table 4.

The double axle bogie was applied in the most onerous location as determined from a series of linear elastic analyses applied incrementally along the span. For Griffith Bridge the centre of the double axle bogie was located 3.13 m from the abutment, coinciding closely with the one third point of the 9.45 m clear span. Due to the humped profile of Greenfield Bridge the axle loading was very unevenly distributed with one axle taking 82% of the load. Therefore the most onerous location was dictated by the heavier axle which was located 0.93 m from the abutment, near to the quarter point of the 4.52 m span; whereas the centre of the bogie was located almost immediately above the abutment. For O'Connell's Bridge, the centre of the bogie was located 3.52 m from the abutment, close to the one third point of the 10.33 m span. These locations were in good agreement with the conventional recommendation that the worst case loading position is located somewhere between the quarter and third span.

The legal load limit was taken as the double axle bogie load required to permit the maximum European road legal vehicle of 40/44 tonne gross vehicle weight (European Parliament and Council of the European Union, 1996). This legal load limit is equal to a 10 tonne allowable axle load (AAL) for a double axle bogie, which after applying the axle factors is equal to a 53 tonne bogie. For Griffith Bridge and Greenfield Bridge the loading at the legal load limit was applied cyclically, loading and unloading to 53 tonnes, until a repeatable response was achieved. For O'Connell's Bridge there was no major change in stiffness in the load deflection response at the legal load limit and therefore cyclic loading was not applied. For the ultimate capacity predictions the loading was applied incrementally in 1 tonne increments until instability occurred and the solution diverged.

6.2 Solution

Although the solution controls for both the experimental service load simulation and the serviceability and ultimate capacity prediction were similar, they are discussed here as they were more critical to the solution at ultimate capacity. A full Newton-Raphson iterative solution, i.e. with the stiffness updated for each iteration of every load increment, using a sparse direct equation solver (ANSYS Inc., 2010) was used. The sparse direct solver was chosen as it is more robust for nonlinear solutions, although it uses significantly more memory than other solvers. Frictional contact elements were used at the contact interface which result in unsymmetrical stiffness matrices. The iterative augmented Lagrange algorithm (Laursen and Simo, 1993) was used for the contact surfaces. This algorithm symmetrizes the matrices allowing less computationally expensive symmetrical solvers to be used. The contact interfaces were initially adjusted to touch, i.e. closing initial gaps and ignoring any initial contact penetration, so that there is no stress at the contact interfaces at the start of the solution. As large loads were being transferred across relatively small contact areas, due to the shallow depths of fill in the models, the contact stiffness was updated at each iteration of the solution to minimise convergence difficulties associated with contact penetration.

As before, an initial gravity step was applied. The double axle load was then applied in 1 tonne increments for each substep. Owing to the large self-weight of the model relative to the live load applied in each substep it was extremely important to determine a force convergence

criterion based on the applied live load only and to exclude the self-weight of the bridge when considering the out of balance loads at the end of each iteration, as otherwise the self-weight would mask a diverging solution. A force convergence tolerance for the out of balance loads equal to 1% of the applied live load increment was applied. This equated to a convergence criterion of 98.1 N for each substep. Up to 50 equilibrium iterations were allowed for each substep. If the substep had not converged after 50 equilibrium iterations the solution was allowed to continue to the next substep, and the solution was monitored to check that the solution converged in subsequent steps. This allowed the solution to progress with both a reasonable load increment and a reasonable number of equilibrium iterations per substep.

6.3 Results

The load deflection responses at the crown centre for each of the bridges are shown in Figure 13, Figure 17 and Figure 20 for loading up to the predicted ultimate capacity limit. For both the full width and half width models, the total factored loads for the double axle bogie are plotted. The development of cracking in the masonry as the load increases is also shown for each of the labelled data points on the load deflection curves. The loads at which the first significant cracks and changes in stiffness were predicted to occur and the lower bound ultimate capacity loads for all of the bridges are summarized in Table 5. For reference, the legal load limit based on the 10 tonne AAL for a double axle bogie is also listed in Table 5.

6.3.1 Griffith Bridge

6.3.1.1 Legal load limit

Examining the load deflection response, as shown Figure 13, at the end of the gravity step some very minor cracking had developed at the base of the spandrel arch interface under the self-weight of the arch. The first cracks developed in the arch barrel at 24 tonnes in the longitudinal direction underneath the wheels of the heavier axle load. The bridge exhibited an approximately linear response up to 32 tonnes. At 34 tonnes a transverse crack formed across the width of the barrel underneath the heavier axle resulting in a change in stiffness in the load deflection response. A plateau in the response can be seen in the load deflection curve preceding the formation of this crack. Cracking at the spandrel arch interfaces and vertical cracking in the parapet walls also occurred at this load. At 40 tonnes transverse cracking

began to develop in the haunch on the loaded side of the arch at the tightest point in the curve. Some minor development of the existing cracks occurred between 40 tonnes and the legal load limit of 53 tonnes.

The unloading of the first cycle and second and third load cycles to 53 tonnes exhibited a repeatable and approximately linear response, indicating that the damage in the bridge had stabilized after the first load cycle. The predicted damage at the legal load limit can be summarized as follows: longitudinal cracking directly in line with the axle load path, some spandrel wall separation, the formation of the first transverse crack or hinge near to the crown and the formation of a second partial hinge across the loaded haunch. Two cycles of loading did not result in further damage propagation. In this sense these cracks could be considered to be active cracks opening and closing under load.

6.3.1.2 Ultimate capacity and failure mechanism

As the loading was increased beyond 53 tonnes, longitudinal cracking at the centreline of the barrel developed at 64 tonnes. The response remained approximately linear until 98 tonnes. At this load, diagonal cracking developed around the heavier axle and the transverse cracking in the haunch extended towards the spandrel walls, leaving intact the interface with the spandrel walls at the tightest point of the curve and cracking around this section. At 102 tonnes diagonal cracking developed in the haunch on the unloaded side of the arch as it was pushed upwards. Further cracking at the spandrel wall interfaces also occurred on the unloaded side of the arch and longitudinal cracks developed in the arch barrel near to the spandrel wall. At 104 tonnes the diagonal cracking on this haunch extended to the centre of the bridge. Beyond this load extensive cracking developed in multiple orientations throughout the masonry material at the crown and haunches and a lower bound solution for the ultimate capacity load was taken as 104 tonnes.

The deflected shape at 104 tonnes is shown in Figure 14 and is similar to that associated with the formation of a four hinge mechanism. However the stiffening effects of the spandrel walls can be seen at the edge of the barrel. Very limited load distribution was provided by the shallow depth of fill and the deflected shape and cracking patterns indicate that the bridge experiences significant three dimensional behaviour giving rise to longitudinal and diagonal cracking with the deflections concentrated underneath the heavier axle load. A plan view of

the crack pattern at 104 tonnes for the full width of the bridge is also shown in Figure 14. It can be seen that at this load, longitudinal cracking has developed underneath each wheel and along the full length of the barrel near the spandrels; cracking has occurred at the arch spandrel interface along the centre section of the span; transverse cracking has developed under the heavier axle load and at the haunch on the loaded side of the arch; and diagonal x-shaped crack patterns have occurred under the heavier axle and on the unloaded haunch. Initially the development of the transverse cracks was similar to that associated with a two dimensional hinge mechanism. However as the loading increased the restraint provided by the spandrel walls resulted in diagonal cracking, initially in the region of loading and subsequently on the unloaded haunch, despite the damage that had occurred at the arch spandrel interface. This resulted in more complex damage than a simple four hinge mechanism, although areas of damage were identified in the region of loading, on the loaded haunch and on the unloaded haunch. This led to failure by local instability of the large sections of masonry surrounding the area immediately under heavier axle load. It should also be noted that the predicted damage in the structure developed concurrently in multiple areas of the structure as the loading approached the ultimate capacity rather than by sequential formation of distinct hinges. No crushing of the masonry material occurred with a maximum predicted compressive stress of 1.8 MPa located immediately under the heavier axle load.

6.3.1.3 Influence of the spandrel walls

To delineate the influence of the spandrel walls on the response of the structure from other three dimensional effects such as transverse load distribution through the fill and transverse bending in the arch barrel the structure was analysed with the spandrel walls removed and restraint applied against outward movement in the normal direction. This assessment was also used to quantify the contribution of the spandrel walls to the ultimate strength of the structure and could also be used to provide a more conservative estimate of the ultimate capacity.

The deflected shape and predicted crack pattern at failure are shown in Figure 15. Although transverse bending and longitudinal cracking do occur, the failure mechanism is that of the classical four hinge mechanism in line with a two dimensional response. However a four hinge mechanism cannot be assumed to occur in the absence of spandrel walls, even in the case of square span arches, as previous experimental studies have shown that, for weaker arches, diagonal crack patterns may form (Wang, 2004). The predicted failure load is 86

tonnes, or an AAL of 16.2 tonnes, indicating that the spandrel walls provided an estimated increase in capacity of 21%.

6.3.1.4 Discussion

Reviewing the axle loads summarized in Table 5, the first crack occurred in the longitudinal direction at 24 tonnes, indicating damage due to transverse bending prior to the formation of any hinges. This occurred under the heavier 15.4 tonne axle of the double axle bogie. Considering working, i.e. unfactored, loads of 10 tonnes per axle, no damage or change in stiffness would be expected to occur. Therefore, under the maximum permitted loads for road legal vehicles the damage that would be anticipated for this bridge ranges from none, for the unfactored working loads, up to the level of damage incurred for the fully factored loads at 53 tonnes, i.e. longitudinal cracking underneath the loading and at the spandrel wall and the formation of two hinges. While the bridge is cracked at this level, there is a significant reserve of strength vis-à-vis the ultimate limit. The predicted ultimate capacity of 104 tonnes equates to an AAL of 19.6 tonnes per axle, nearly double the 10 tonne AAL service load requirement. A change in the stiffness response did not occur until the formation of the first transverse crack, i.e. the first hinge, occurred at 34 tonnes or approximately one third of the ultimate capacity load.

The restraint provided by the spandrel walls resulted in more complex damage than a simple four hinge mechanism. Despite the damage that had occurred at the arch spandrel interface, the spandrel walls were shown to provide a substantial increase in capacity of 21%.

6.3.2 Greenfield Bridge

6.3.2.1 Legal load limit

Again the loading was applied in a series of load cycles at the legal load limit. However, unlike Griffith Bridge, a repeatable linear response was not exhibited after the initial loading as is shown in Figure 16. Cracking was first initiated under the heavier axle load at 38 tonnes as a transverse crack which developed steadily out towards the spandrel walls under increasing load. Just below the legal load limit of 53 tonnes, a transverse crack developed along the springing on the loaded side of the structure at 52 tonnes. No further cracking developed between this and 53 tonnes and the final crack pattern for load cycle 1 is shown in

Figure 16. The bridge was then cyclically unloaded and reloaded to 53 tonnes with further cracking developing along the spandrel wall interface at each load cycle until the damage at the legal load limit stabilized.

Examining the load deflection response for the ultimate capacity loading in Figure 17, it can be seen that cracking at the spandrel walls and a change of stiffness occur at 55 tonnes, i.e. just above the 53 tonne legal load limit. Comparing the crack patterns at the end of load cycle 1 and load cycle 5 from the service level analysis at 53 tonnes to the crack pattern from the ultimate capacity analysis at 55 tonnes, Figure 18, it can be seen that damage accrues incrementally under the load cycles at 53 tonnes until it reaches the same level of damage as predicted for 55 tonnes.

6.3.2.2 Ultimate capacity and failure mechanism

The progressive development of cracking up to failure is shown in Figure 17 and a plan view of the crack pattern at the ultimate capacity load is shown in Figure 19. Diagonal and transverse cracking has occurred on both the loaded and unloaded haunches and transverse cracks have formed along the springing line of either abutment, effectively the formation of four hinges in the arch barrel leading to instability in the longitudinal direction. Greenfield Bridge demonstrated significant transverse capacity with the majority of damage occurring in the transverse or diagonal direction. Extensive damage occurred at the spandrel walls and outward movement was predicted in the parapets which were not restrained by the wing walls, as can be seen in the deflected shape of the bridge shown in Figure 19, indicating possible instability of the parapets approaching ultimate capacity failure. The predicted failure mechanism of the bridge is a hinge mechanism failure of the barrel, albeit with diagonal rather than transverse cracking, at a lower bound failure load of 167 tonnes or an AAL of 31.5 tonnes. A maximum compressive stress of 2.14 MPa was predicted immediately under the heavier axle load and no crushing behaviour in the model occurred.

6.3.2.3 Discussion

For Greenfield Bridge it was found that there was potential for significant cracking to occur under service level loads, as was the case with Griffith Bridge. However, for Greenfield Bridge a number of load cycles were required at the legal load limit for the damage in the structure to stabilize, with the cracks tending to propagate along the spandrel wall interface

and across the width of the arch, demonstrating progressive damage in the bridge under repeated loads at the legal load limit. This differed from Griffith Bridge for which a repeatable response occurred after the first load cycle. The formation of two hinges and separation at the spandrel walls was predicted under the repeated application of loads at the legal limit. However, despite this level of damage there is a significant reserve in strength, with ultimate capacity failure predicted to occur at over three times the legal load limit.

In a similar manner to Griffith Bridge, the change in the stiffness response of the structure occurred at approximately one third of the ultimate capacity load. Owing to the humped profile of the vertical alignment, the bogie load was very unevenly distributed across the two axles. For a humped profile road the respective sum total load factors for each axle is 4.35 and 0.95, resulting in 82% of the bogie load being applied to the critical axle, i.e. 137.1 tonnes in the case of Greenfield Bridge, indicating a very high capacity bridge.

The comparison between the experimental responses and the finite element simulations of the in-situ testing had suggested that there was existing damage in the structure at the spandrel wall interface. This was further corroborated by the analysis carried out at the legal load limit which also predicted damage at the spandrel wall interface.

6.3.3 O'Connell's Bridge

6.3.3.1 Legal load limit and ultimate capacity predictions

The load deflection response and crack patterns for O'Connell's Bridge are shown in Figure 20. As there was no significant change in stiffness at the legal load limit, cyclic loading was not applied. At 80 tonnes cracking in plane with the intrados/extrados of the arch developed at the centreline of the bridge in the region of the heavier axle load indicating localized material failure in the loading region and this load was taken as the lower bound ultimate capacity load, i.e. an AAL of 15.1 tonnes. Again no crushing of the masonry material occurred with a maximum compressive stress of 0.58 MPa under the heavier axle load. O'Connell's Bridge is of random rubble construction with large mortar joints and as such was assigned lower material property values compared with Griffith Bridge and Greenfield Bridge. Correspondingly, the results of the analysis showed that it exhibited significantly different behaviour to the other two structures considered. The predicted failure mechanism was by localized material failure under the load which was accompanied by extensive

longitudinal cracking due to transverse bending in the arch barrel, as shown in Figure 21. The formation of longitudinal cracking in the arch barrel was initiated at 20 tonnes distributed across a 12.8 tonne axle and a 7.2 tonne axle which is close to working load levels for road legal vehicles and certainly within the range of commonly encountered overloaded vehicles. O'Connell's Bridge exhibited longitudinal cracking of the arch barrel as shown in Figure 4 under previous loading conditions, and this damage is replicated in the finite element model under realistic axle loads that the structure could be expected to encounter.

6.3.3.2 The influence of the depth of fill

Increasing the depth of fill on an arch is a commonly proposed as a remedial strengthening measure, as the increased dead load provides additional longitudinal restraint and the increased depth allows for greater load distribution. However, if the three dimensional response of the structure is considered, the additional dead load would also be expected to increase the transverse bending in the arch which may negate the purported benefits. As O'Connell's bridge demonstrated damage due to transverse bending it was decided to investigate the effect of an additional 0.610 m of fill on the structure.

The contact pressures at the interface between the fill and the masonry at 80 tonnes are shown for both depths of fill, 0.100 m and 0.710 m at the crown, in Figure 22. The pressure applied to the surface of the fill for the wheel of the heavier axle is 2.8 MPa. For the shallower depth of fill the maximum contact pressure is 2.6 MPa indicating that very limited load distribution occurs. However, for the increased depth of fill the maximum contact pressure decreases to 0.45 MPa.

The predicted failure mechanism for the model with the increased depth of fill was by lateral failure of the parapet walls at 124 tonnes. The deflected shape showing the movement of the parapet walls and the crack pattern at 124 tonnes are shown in Figure 23. The load deflection response at the centre of the parapet, rather than the crown centre, is shown in Figure 24, demonstrating that large deflections occurred in the parapet immediately prior to failure between 122 and 124 tonnes. This was accompanied by extensive longitudinal cracking distinct from the longitudinal cracks formed under the axle load due to transverse bending. The increased load distribution provided by the depth of fill prevented localized material failure under the load and increased the capacity of the arch by approximately 50%.

Longitudinal cracking still developed in the barrel due to transverse bending although there was an increase in the load at which this occurred of 30%, with the first cracks occurring at 26 tonnes, demonstrating that an increased capacity may be achieved with additional fill even where the transverse capacity is a concern.

7 Discussion

Incremental loading and progressive development of cracking in the structure allow for the structural response and associated damage to be considered for all levels of loading and a wide range of varying scenarios. However, the most useful application of the three dimensional nonlinear finite element models is to understand the expected damage under service level loads. At the moment the focus of assessment is on ultimate capacity assessment only. This provides very limited information where, for example, existing damage has occurred within the assessed capacity loading. The significance of assessment at the serviceability level will be dependent, in large part, on the expected loading for the bridge in question. In the absence of significant levels of damage, ultimate capacity assessment will generally be satisfactory for assessing gross vehicle weight limits for bridges that are subject to the odd illegally loaded vehicle. More useful applications for serviceability level assessment, where the effort is more likely to be justified, would be for proposed heavy load routes subject to high volume traffic or for bridges exhibiting high levels of damage, where assessed ultimate capacities provide limited information or reassurance.

For all three of the bridges considered, significant cracking occurred at the legal load limit and the initiation of damage was predicted at approximately a quarter of the ultimate capacity load, with significant changes in stiffness at approximately one third the ultimate capacity load for Griffith Bridge and Greenfield Bridge. The repeated application of loads at the legal load limit demonstrated that cracks could either be active, i.e. opening and closing under loading, or propagating, with incremental damage occurring under the repeated application of the loads. This also allowed for a stable level of damage to be determined, thereby identifying a level of damage associated with the legal load limit. This type of information could influence the course of action to be taken to address existing damage, e.g. the use of flexible filler to prevent water damage rather than strengthening with brittle materials, or could be used to identify if damage is attributable to legal loads or excess loads.

Despite damage occurring at or close to the legal load limit, a significant reserve in strength was predicted with ultimate capacities between 1½ to 3 times the legal load limit. The ultimate capacity predictions for the three bridges presented in this paper were all above the allowable axle load requirement of 10 tonnes for a double axle bogie for road legal vehicles up to a gross vehicle weight of 40/44 tonnes. While a large reserve in strength is present beyond the initiation of damage, the development of cracks under service loads will lead to accelerated deterioration of the structure and will be exacerbated by other mechanisms such as weathering, freeze thaw action and vegetation growth, in addition to altering the stiffness response of the structure.

For all of the bridges, brittle failures under very small deflections were predicted, with extensive cracking developing prior to failure. However, the development of damage and the failure mechanisms varied: Griffith Bridge and Greenfield Bridge exhibited higher transverse capacities and the development of diagonal rather than transverse hinges owing to the restraint of the spandrel walls, whereas O'Connell's Bridge demonstrated severe longitudinal cracking and localized material failure in the loading region.

The damage patterns for all of the structures were influenced by the three dimensional response. Varying degrees of longitudinal cracking were predicted for all of the bridges including the analyses of Griffith Bridge with the spandrel walls removed and O'Connell's Bridge with the additional depth of fill. Extensive longitudinal cracking was predicted for O'Connell's Bridge which could not be accounted for with a two dimensional model. For Griffith Bridge the diagonal cracking was shown to be caused by the stiffening effect of the spandrel walls.

Cracking at the arch spandrel interface was predicted in all of the structures prior to failure. Due to the unknown load history of the structure it may be sensible to neglect the contribution of the spandrel walls altogether in determining an ultimate capacity failure load. However, the stiffening effects of the spandrel walls are important in terms of capturing the actual response of the structure as was demonstrated by the service and high level load simulations and by the ultimate capacity assessments with and without the spandrel walls for Griffith Bridge.

The inclusion of the fill material in the model is an extremely important parameter, providing load distribution and transfer to the arch barrel as well as additional restraint. All of the bridges presented in this paper had very shallow depths of fill ranging from only 100 mm to 126 mm at the crown, resulting in depths of fill of 150 mm to 250 mm underneath the heavier axle of the double axle bogie. The shallow depths of fill limited the extent to which the applied load was distributed in the ultimate capacity predictions and consequently the initial cracking for all of the bridges was highly localized to the heavier axle of the double bogie. The load distributions for the moving vehicle simulation for Griffith Bridge demonstrated how the depth of fill determined whether the load transferred to the arch was effectively a patch load or full width load, leading to differing load scenarios at the abutments, haunch and crown. For O'Connell's Bridge two different depths of fill were considered, keeping the load location fixed, and it was demonstrated that the additional load dispersion increased the predicted ultimate capacity by approximately 50%, despite the limited transverse capacity in the barrel. However, the additional fill did not lead to a four hinge type mechanism failure and it was demonstrated that even for greater depths of fill the transverse behaviour still requires to be considered.

8 Conclusions

Nonlinear finite element models were validated at service load levels, high load levels and against in-situ damage, successfully reproducing three dimensional behaviour under a wide range of loading conditions. The finite element models were then used to assess behaviour at the legal load limit and predict lower bound ultimate capacity failure loads and mechanisms. The modelling techniques employed captured the load dispersion through the fill, the transfer of load from the fill to the arch barrel, frictional sliding between the fill and the masonry, the transverse behaviour of the arch, the stiffening effects of the spandrel walls, the nonlinear behaviour of the materials, initiation and progressive development of cracking in the structure, and allowed for consideration of multiple causes of failure such as extensive diagonal cracking, transverse failure, localized material failure, hinge mechanism failure and the overturning of parapet walls. The influence of the fill material and the spandrel walls on the response of the structure was investigated, and comparisons with experimental service and high level load deflections were used to identify pre-existing damage.

Significant damage was identified at the legal load limit, however it was also found that there is a large reserve in capacity prior to failure. It was demonstrated that cracks may be active or

propagating under service level loads, but that a stable level of damage may be identified for a given load. Given that masonry arch bridges frequently exhibit signs of damage under working loads and are unlikely to be loaded in the ultimate capacity range owing to their high capacities, it is concluded that assessment of masonry arch bridges needs to focus on service level loading and the subtleties of the three dimensional response.

Acknowledgements

The authors gratefully acknowledge the National Roads Authority of Ireland for funding this research under the National Roads Authority Research Fellowship Programme.

References

ANSYS Inc. (2010) *ANSYS Help Manual*, Canonsburg, PA.

Behnamfar, F. and Afshari, M. (2013) Collapse analysis and strengthening of stone arch bridges against earthquake, *International Journal of Architectural Heritage*, 7(1) 1-25.

Boothby, T.E., Domalik, D.E. and Dalal, V.A. (1998) Service load response of masonry arch bridges, *Journal of Structural Engineering*, 124(1) 17-23.

Boothby, T.E. and Fanning, P.J. (2004) Load rating of masonry arch bridges: refinements, *Journal of Bridge Engineering*, 9(3) 304-307.

Callaway, P., Gilbert, M. and Smith, C.C. (2012) Influence of backfill on the capacity of masonry arch bridges, *Proceedings of the Institution of Civil Engineers – Bridge Engineering*, 165(3) 147-157.

Castigliano, A. (1879) *Théorie de l'équilibre des systèmes élastiques et ses applications*, Turin.

Cavicchi, A. and Gambarotta, L. (2007) Lower bound limit analysis of masonry bridges including arch–fill interaction, *Engineering Structures*, 29(11) 3002-3014.

Crisfield, M.A. (1985) *Finite element and mechanism methods for the analysis of masonry and brickwork arches, Research Report 19*, Transport and Road Research Laboratory, London, HMSO.

Crisfield, M.A. and Packham, A.J. (1987) *A mechanism program for computing the strength of masonry arch bridges, Research Report 124*, Transport and Road Research Laboratory, London, HMSO.

Davy, N. (1953) *Tests on Road Bridges, National Building Studies Research Paper No. 16*, London, HMSO.

Delbecq, J.M. (1982) Analyse de la stabilité des voûtes en maçonnerie par le calcul à la rupture, *Journal de Mécanique Théorique et Appliqué*, 1(1) 91-121.

Drucker, D. C. and Prager, W. (1952) Soil mechanics and plastic analysis for limit design, *Quarterly of Applied Mathematics*, 10(2) 157–165.

European Parliament and Council of the European Union. Directive 1996/53/EC of the European Union and of the Council of 25 July 1996 laying down for certain road vehicles circulating within the Community the maximum authorized dimensions in national and international traffic and the maximum authorized weights in international traffic. *Official Journal of the European Communities*, L235, 17.9.1996, 59-75.

Fairfield, C.A. and Ponniah, D.A. (1994) Model tests to determine the effect of fill on buried arches, *Proceedings of the Institution of Civil Engineers – Structures and Buildings*, 104(4) 471-482.

Fanning, P.J. and Boothby, T.E. (2001) Three-dimensional modelling and full-scale testing of stone arch bridges, *Computers and Structures*, 79(29-30) 2645-2662.

Fanning, P.J. and Boothby, T.E. (2005) *Service and high level load testing Greenfields Bridge*, Dublin, Bridge Research Group University College Dublin.

Fanning, P.J., Sobczak, L., Boothby, T.E. and Salamoni ,V. (2005) Load testing and model simulations for a stone arch bridge, *Bridge Structures*, 1(4) 367-378.

Gibbons, N. (2014) *Modelling and assessment of masonry arch bridges*, Doctor of Philosophy thesis, University College Dublin.

Gilbert, M. and Melbourne, C. (1994) Rigid-block analysis of masonry structures. *The Structural Engineer*, 72(21) 356-361.

Harvey, W.J. (1988) Application of the mechanism analysis to masonry arches. *The Structural Engineer*, 66(5) 77-84.

Harvey, W.J., Vardy, A.E., Craig, R.F., and Smith, F.W. (1989) *Load tests on a full scale model four metre span masonry arch bridge, Contractor Report 155*, Transport and Road Research Laboratory, London, HMSO.

Hendry, A.W. (1990) *Masonry properties for assessing arch bridges, Contractor Report 244*, Transport and Road Research Laboratory, London, HMSO.

Hendry, A.W., Davies, S.R. and Royles, R. (1985) *Test on stone masonry arch at Bridgemill - Girvan, Contractor Report 7*, Transport and Road Research Laboratory, London, HMSO.

Hendry, A.W., Davies, S.R., Royles, R., Ponniah, D.A., Forde, M.C. and Komeyli-Birjandi, F. (1986) *Load test to collapse on a masonry arch bridge at Bargower, Strathclyde, Contractor Report 26*, Transport and Road Research Laboratory, London, HMSO.

Heyman, J. (1966) The stone skeleton, *International Journal of solids and structures*, 2(2) 249-279.

Heyman, J. (1982) *The masonry arch. Chichester*, Ellis Horwood.

Highways Agency (1997) BA 16/97 The Assessment of Highway Bridges and Structures. *Design Manual for Roads and Bridges*, Volume 3, Section 4, Part 4, London, HMSO.

Highways Agency (2001) BD 21/01 The Assessment of Highway Bridges and Structures, *Design Manual for Roads and Bridges*, Volume 3, Section 4, Part 3, London, HMSO.

Hodgson, J.A. (1996) *The behaviour of skewed masonry arch bridges*, Doctor of Philosophy thesis, University of Salford.

Hughes, T.G., Davies, M.C.R. and Taunton, P.R. (1998) Small scale modelling of brickwork arch bridges using a centrifuge, *Proceedings of the Institution of Civil Engineers – Structures and Buildings*, 128(1) 49-58.

Hughes, T.G., Hee, S.C. and Soms, E. (2002) Mechanism analysis of single span masonry arch bridges using a spreadsheet. *Proceedings of the Institution of Civil Engineers – Structures and Buildings*, 152(4) 341-350.

Kooharian A. (1952) Limit analysis of voussoir (segmental) and concrete arches. *Proceedings of the American Concrete Institute*, 24(4), 317–328.

Laursen, T.A. and Simo, J.C. (1993) Algorithmic Symmetrization of Coulomb Frictional Problems Using Augmented Lagrangians, *Computer Methods in Applied Mechanics and Engineering*, 108(1-2) 133-146.

Melbourne, C. and Gilbert, M. (1995) The behaviour of multiring brickwork arch bridges, *The Structural Engineer*, 73(3) 39-47.

Melbourne, C., Gilbert, M. and Wagstaff, M. (1997) The collapse behaviour of multispan brickwork arch bridges, *The Structural Engineer*, 75(17) 297-305.

Melbourne, C. and Walker, P.J. (1990) *Load test to collapse on a full scale model six metre span brick arch bridge*, *Contractor Report 189*, Transport and Road Research Laboratory, London, HMSO.

Milani, G. and Lourenço, P. B. (2012) 3D non-linear behavior of masonry arch bridges. *Computers & Structures*, 110-111, 133-150.

National Roads Authority (2009) *Stage I Assessment Methodology Report*, Dublin, National Roads Authority.

Navier, C.L.M.H. (1826) *Résumé des leçons données à l'école royale des ponts et chaussées sur l'application de la mécanique à l'établissement des constructions et des machines*, Paris, Didot Pere et Fils.

Network Rail (2006) *The Structural Assessment of Underbridges, Guidance Note NR/GN/CIV/025*, London, Network Rail.

Ng, K.H. (1999) *Analysis of masonry arch bridges*, Doctor of Philosophy thesis, Napier University, Edinburgh.

Page, J. (1987) *Load tests to collapse on two arch bridges at Preston, Shropshire and Prestwood, Staffordshire, Research Report 110*, Transport and Road Research Laboratory, London, HMSO.

Page, J. (1988) *Load tests to collapse on two arch bridges at Torksey and Shinafoot, Research Report 159*, Transport and Road Research Laboratory, London, HMSO.

Page, J. (1989) *Load tests to collapse on two arch bridges at Strathmashie and Barlae, Research Report 201*, Transport and Road Research Laboratory, London, HMSO.

Page, J. (1993) *Masonry arch bridges: state of the art review*, Transport and Road Research Laboratory, London, HMSO.

Page, J. (1995) Load tests for assessment of in-service arch bridges, *Arch Bridges: Proceedings of the First International Conference on Arch Bridges*, 3-6 September, Melbourne, C. (Ed.) 299-308, Bolton.

Pippard, A.J.S. (1948) The approximate estimation of safe loads on masonry bridges, *The Civil Engineer in War*, 1, 365-372.

Pippard, A.J.S. and Ashby, R.J. (1939) An Experimental Study of the Voussoir Arch, *Journal of the Institution of Civil Engineers*, 10, 383-405.

Ponniah, D.A. and Prentice, D.J. (1998) Load-carrying capacity of masonry arch bridges estimated from multi-span model tests, *Proceedings of the Institution of Civil Engineers Structures and Buildings*, 128(1) 81-90.

Rafiee, A., Vinches, M. and Bohatier, C. (2008) Application of the NSCD method to analyse the dynamic behaviour of stone arched structures, *International Journal of Solids and Structures*, 45(25) 6269-6283.

Rankine, W.J.M. (1858) *A Manual of Applied Mechanics*, London, Charles Griffin & Co.

Robinson, D.J., Johnston, R. and Taylor S.E. (2010) Finite element analysis of a skewed flexi-arch, *Proceedings of the Bridge and Concrete Research Ireland Joint Symposium*, 505-512, Cork.

Royles, R. and Hendry, A.W. (1991) Model tests on masonry arches, *Proceedings of the Institution of Civil Engineers*, 91(2) 299-321.

Sustainable Bridges (2007) *Demonstration bridge C: masonry arch structure, Background document SB7.4*, Sustainable Bridges, EU FP6.

Tao, H. (2003) *The behaviour of open spandrel brickwork masonry arch bridges*, Doctor of Philosophy thesis, University of Salford.

Towler, K.D.S. (1981) *The structural behaviour of brickwork arches*, Doctor of Philosophy thesis, University of Liverpool.

Wang, J. (2004) *The three dimensional behaviour of masonry arches*, Doctor of Philosophy thesis, University of Salford.

Willam, K.J. and Warnke, E.P. (1975) Constitutive model for the triaxial behavior of concrete, *International Association for Bridge and Structural Engineering (Italian*

Group) and Istituto Sperimentale Modelli e Strutture Seminar on Concrete Structures subjected to Triaxial Stresses 1974, 19, 174-179, Bergamo, Italy.

Yang, Y. (1991) *Progressive failure analysis of masonry arch bridges*, Doctor of Philosophy thesis, University of Wollongong.

Young, T. (1817) Bridge, *Supplement to the fourth, fifth and sixth editions of the Encyclopaedia Britannica*, 497-520, Edinburgh, Archibald Constable & Co.

Tables

Table 1 Bridge dimensions

	Griffith Bridge	Greenfield Bridge	O'Connell's Bridge
span [m]	9.45	4.52	10.33
rise [m]	2.71	1.10	3.30
ring thickness [m]	0.446	0.465	0.610
depth of fill [m]	0.126	0.126	0.100
width [m]	7.84	7.50	6.77

Table 2 Material properties

	Griffith Bridge	Greenfield Bridge	O'Connell's Bridge
Masonry			
E [GPa]	10	15	4
ν	0.3	0.3	0.3
ρ [kg/m³]	2200	2200	2324
f_c [MPa]	10.0	12.0	7.6
f_t [MPa]	0.5	0.7	0.25
f_{cb} [MPa]	12.0	14.4	9.1
f_1 [MPa]	14.5	17.4	11.0
f_2 [MPa]	17.3	20.7	13.1
β_t	0.01	0.01	0.01
β_c	0.01	0.01	0.01
Fill			
E [GPa]	0.5	0.5	0.5
ν	0.23	0.23	0.23
ρ [kg/m³]	1700	1700	1700
c [Pa]	1000	1000	1000
ϕ [deg]	44.43	44.43	44.43
ϕ_f [deg]	44.43	44.43	44.43
Masonry fill interface			
μ	0.2	0.2	0.2

Table 3 Axle loads for service load tests

[tonnes]	Griffith Bridge	Greenfield Bridge
axle 1	5.25	14.1
axle 2	5.25	15.7
axle 3	10.55	15.7
axle 4	10.55	–
Total	31.6	45.5

Table 4 Partial load factors for ultimate capacity assessment

	Critical axle	Other axle
Double axle	3.4	1.9
Double axle with axle lift-off	4.35	0.95

Table 5 Predicted loads for initiation of damage, change in stiffness and ultimate capacity

	AAL per axle [tonnes]	lighter axle [tonnes]	heavier axle [tonnes]	total factored load [tonnes]
Griffith Bridge				
initiation of damage	4.5	8.6	15.4	24
change in stiffness	6.4	12.2	21.8	34
legal load limit	10.0	19.0	34.0	53
ultimate capacity	19.6	37.3	66.7	104
Greenfield Bridge				
initiation of damage	7.2	6.8	31.2	38
change in stiffness	9.8	9.3	42.7	52
legal load limit	10.0	9.5	43.5	53
ultimate capacity	31.5	29.9	137.1	167
O'Connell's Bridge				
initiation of damage	3.8	7.2	12.8	20
change in stiffness	3.8	7.2	12.8	20
legal load limit	10.0	19.0	34.0	53
ultimate capacity	15.1	28.7	51.3	80

Figures

Figure 1 Griffith Bridge

Figure 2 Greenfield Bridge

Figure 3 O’Connell’s Bridge

Figure 4 Longitudinal cracking of arch barrel in O'Connell's Bridge

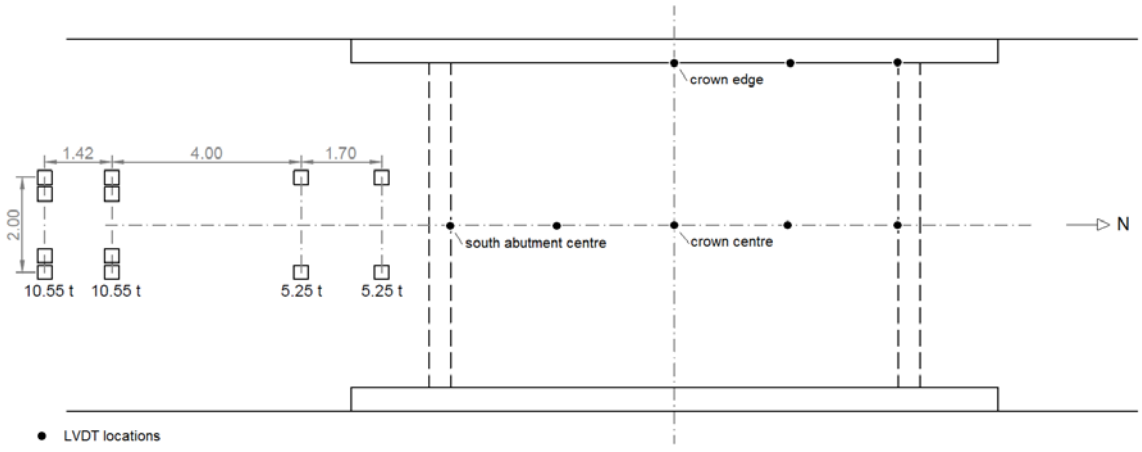

Figure 5 Axle configuration and LVDT locations for service load testing of Griffith Bridge

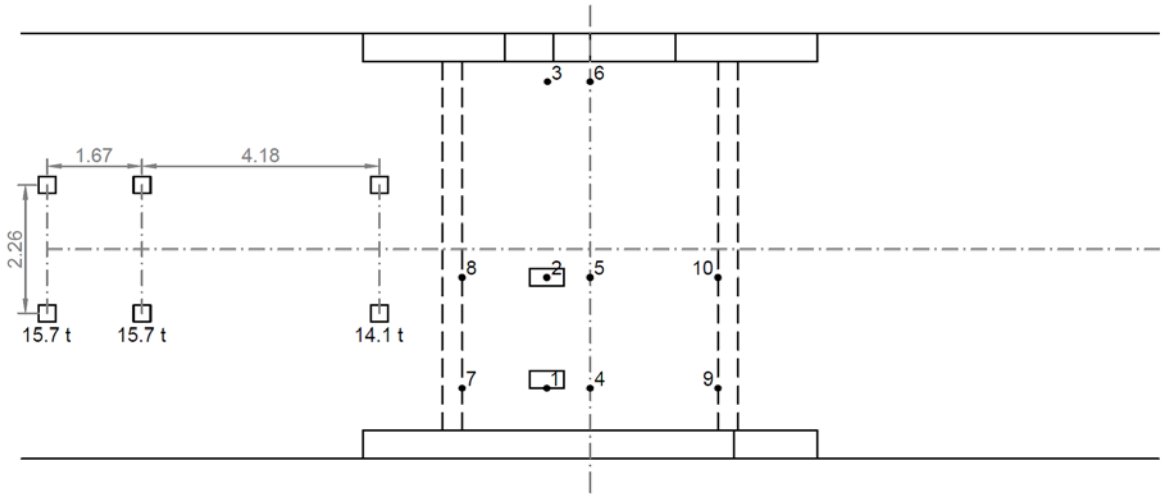

Figure 6 LVDT locations, axle configuration for service load testing and patch load locations for high level load tests for Greenfield Bridge

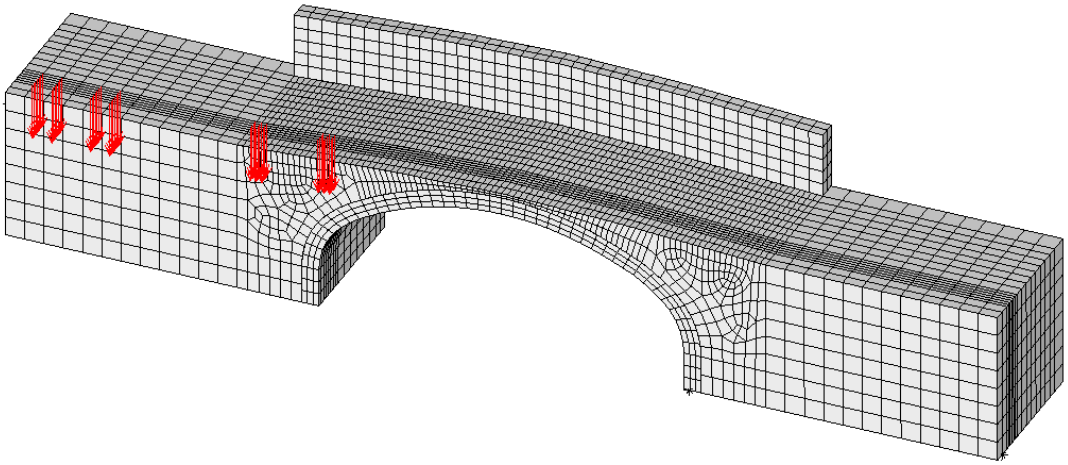

Figure 7 Finite element mesh for half model of Griffith Bridge

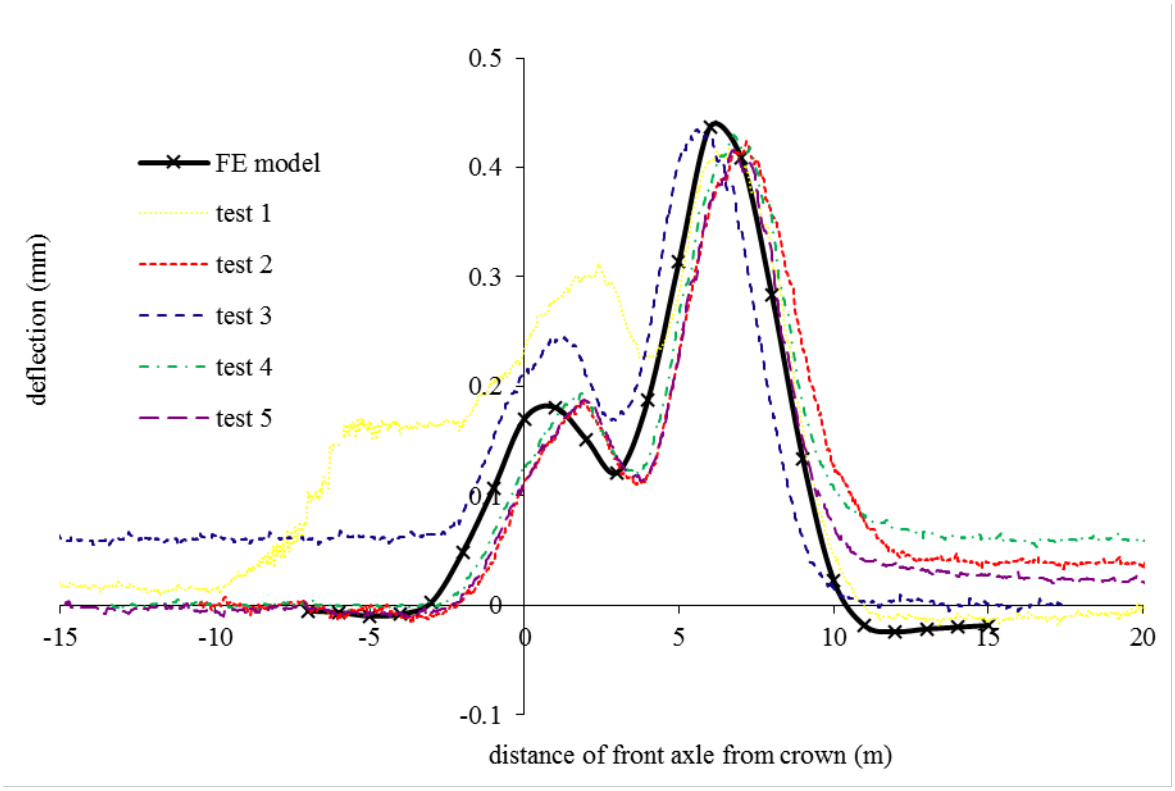

Figure 8 Load deflection response for Griffith Bridge at crown centre

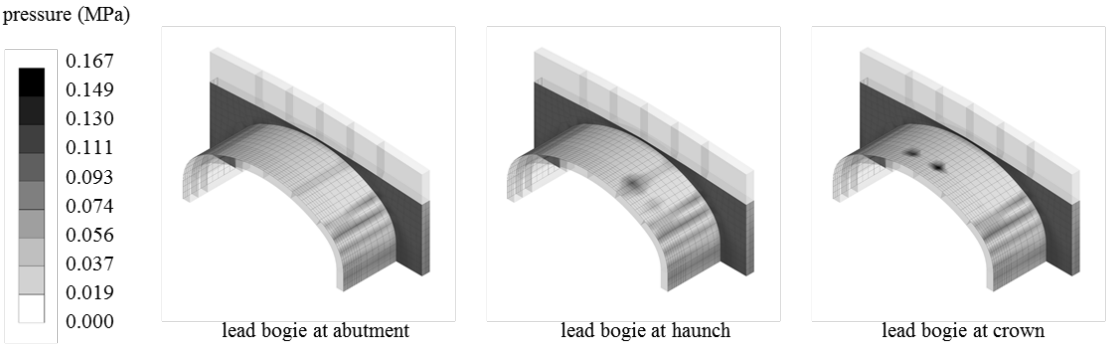

Figure 9 Contact pressure for service load vehicle on Griffith Bridge

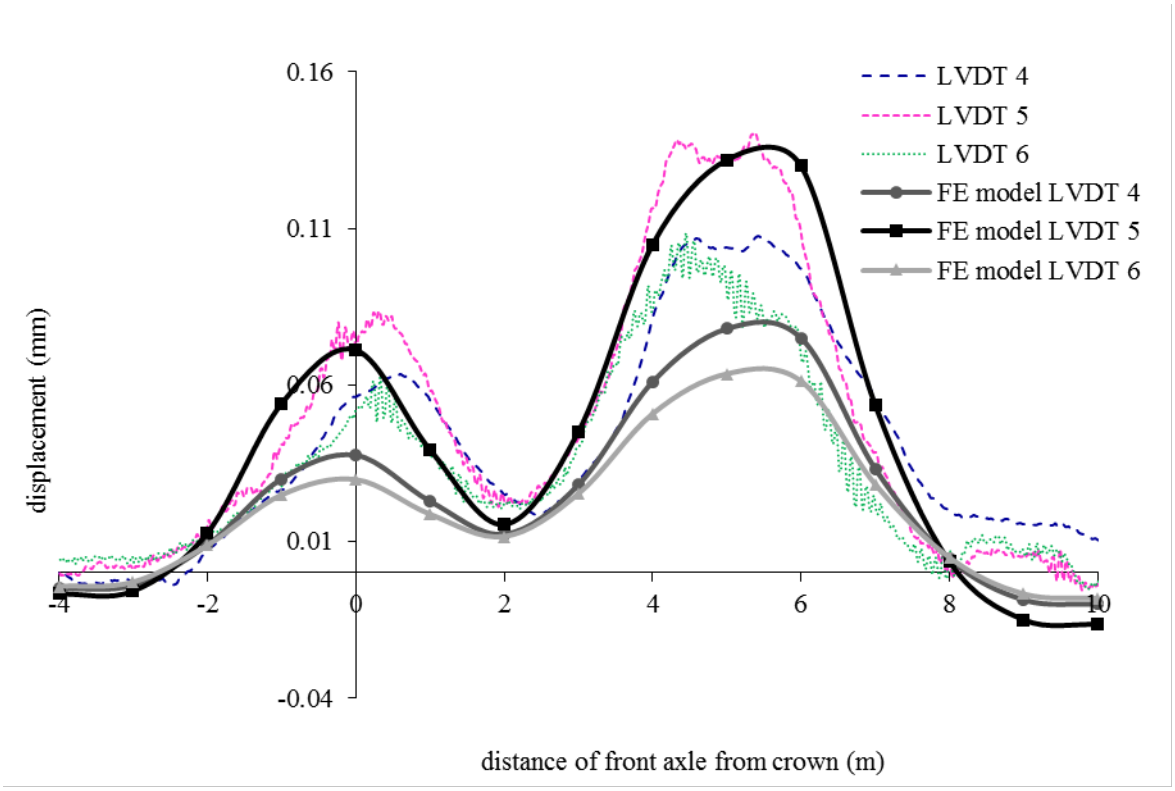

Figure 10 Load deflection response for Greenfield Bridge along the line of the crown

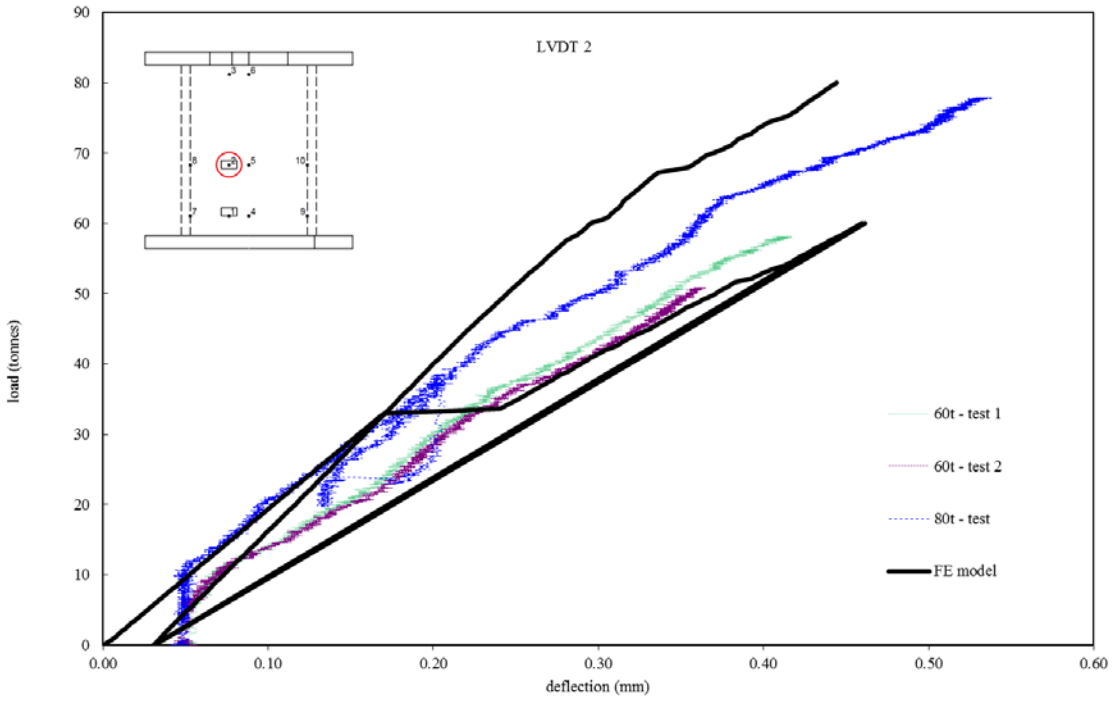

Figure 11 Load deflection response for high level load test for Greenfield Bridge

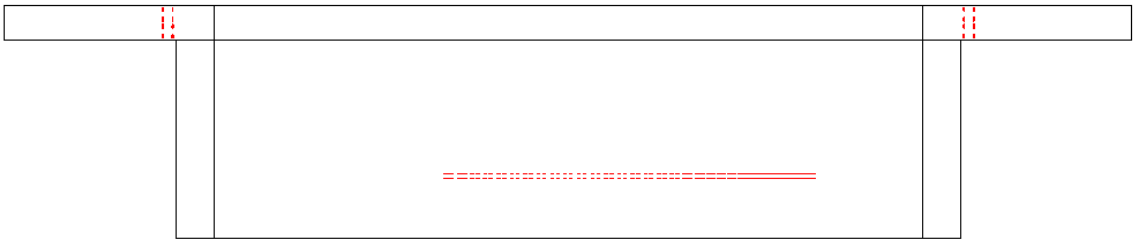

Figure 12 Longitudinal cracking in O'Connell's Bridge at 20 tonnes

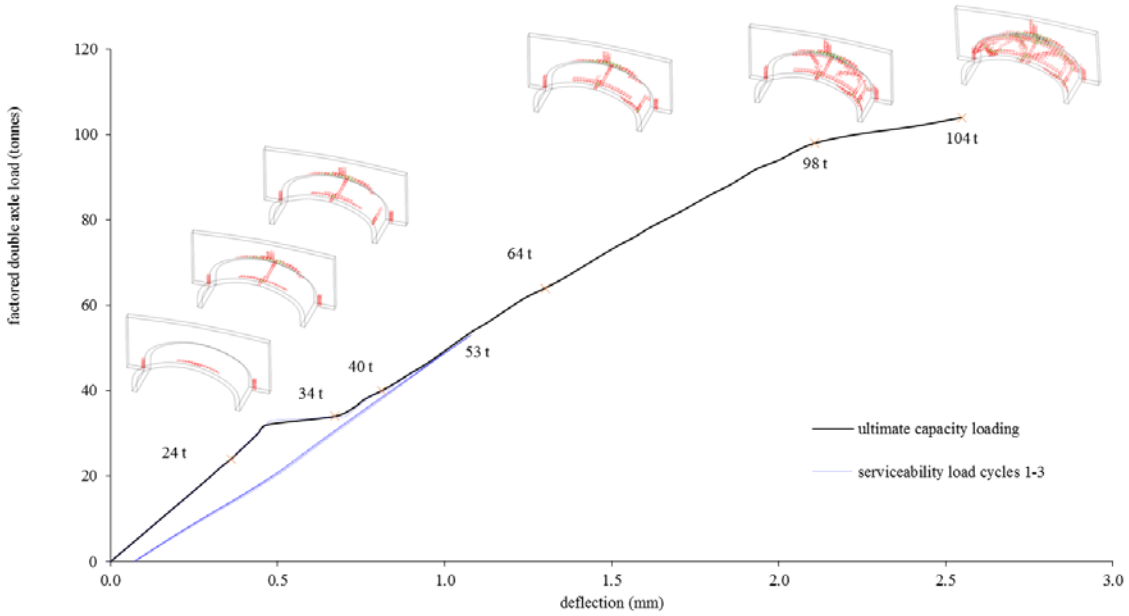

Figure 13 Load deflection response at crown centre for Griffith Bridge

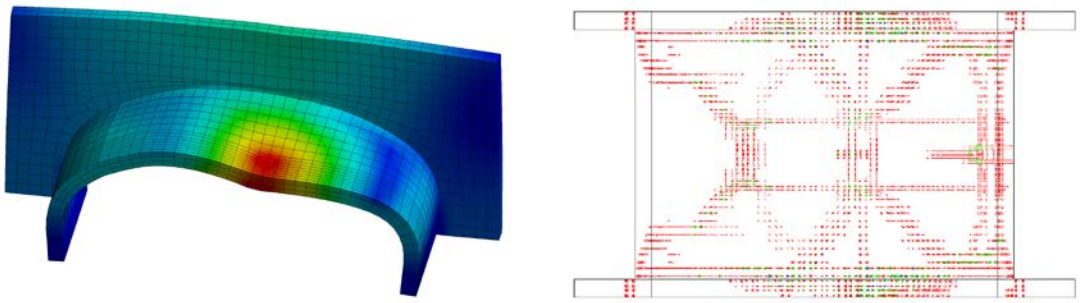

Figure 14 Scaled deflected shape and crack pattern at 104 tonnes for Griffith Bridge

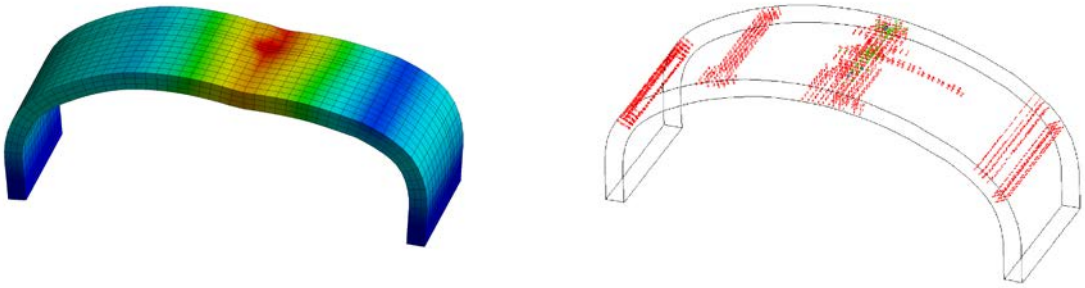

Figure 15 Scaled deflected shape and crack pattern at 86 tonnes for Griffith Bridge without spandrel walls

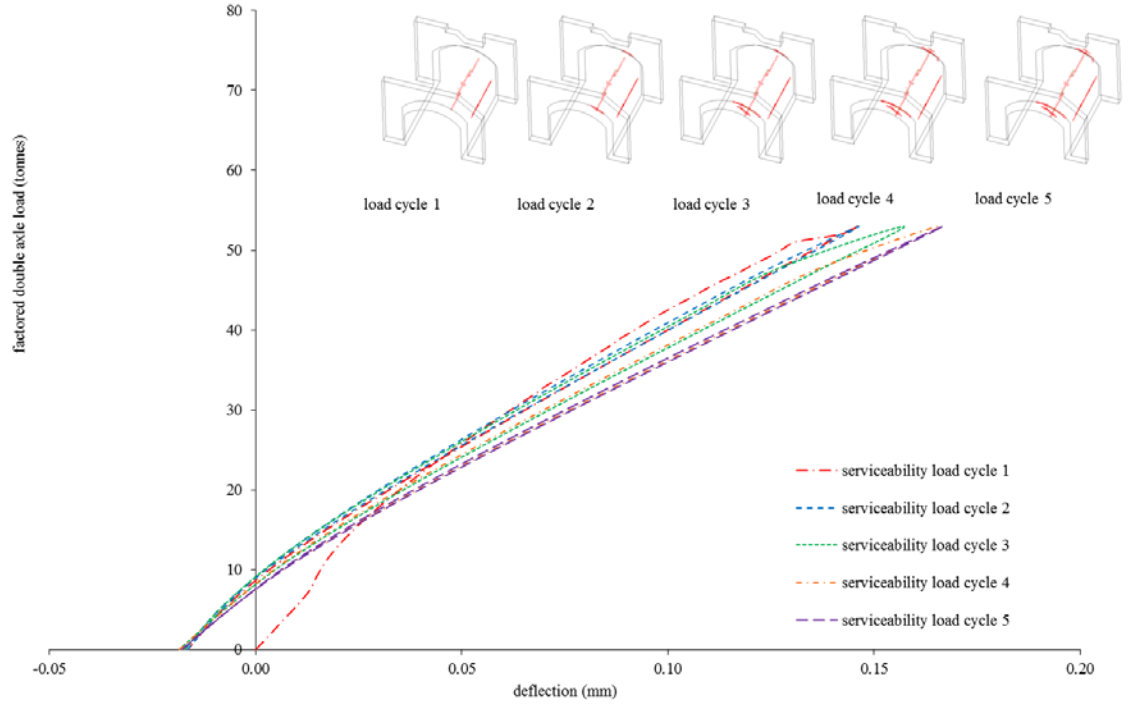

Figure 16 Load deflection response at crown centre for cyclic loading at the legal load limit for Greenfield Bridge

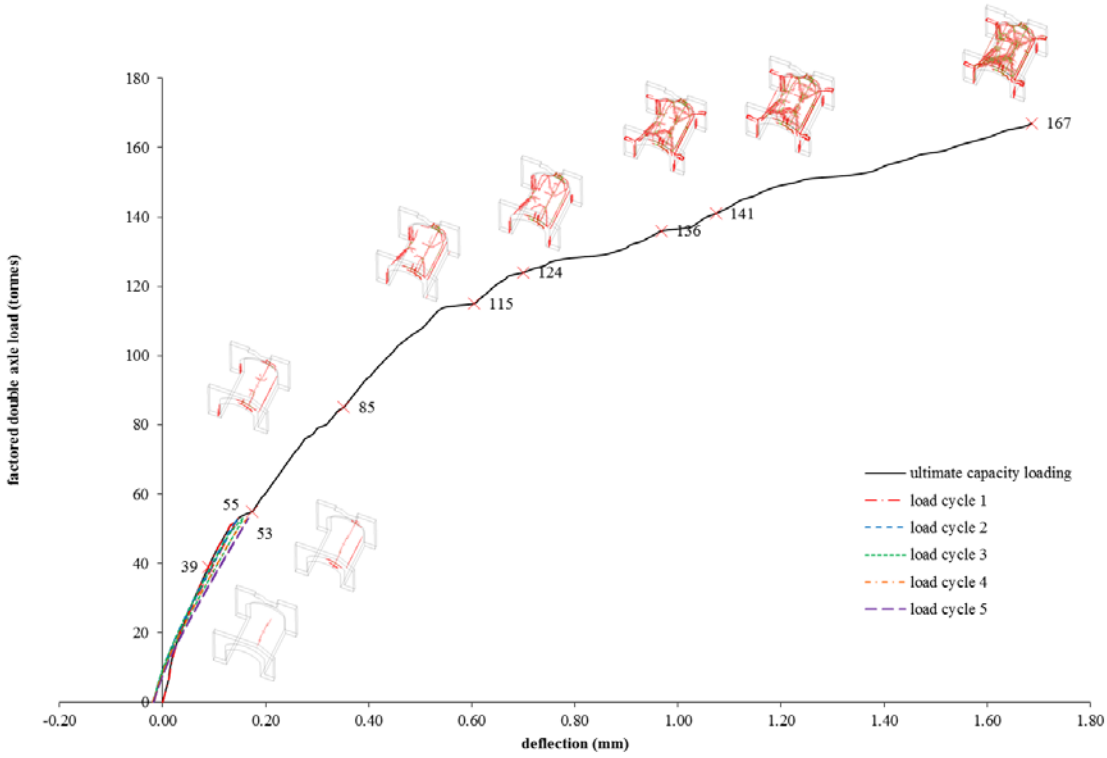

Figure 17 Load deflection response at crown centre of Greenfield Bridge

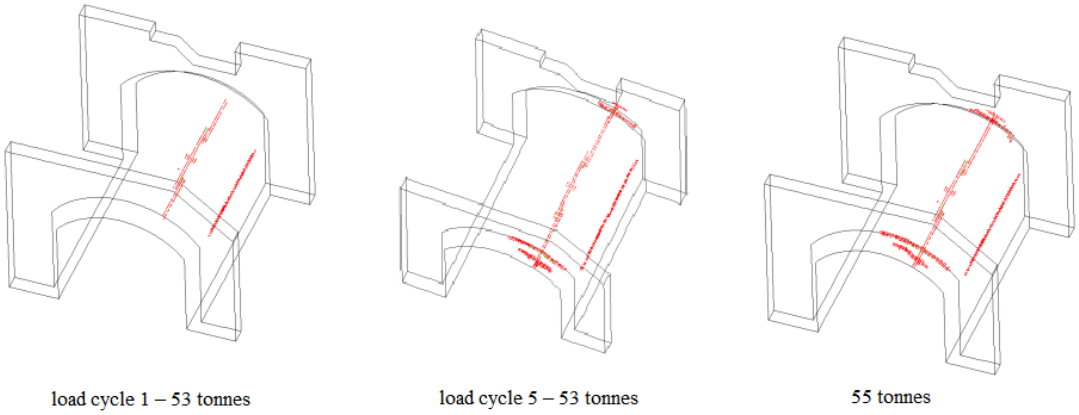

Figure 18 Crack patterns at 53 tonnes and 55 tonnes

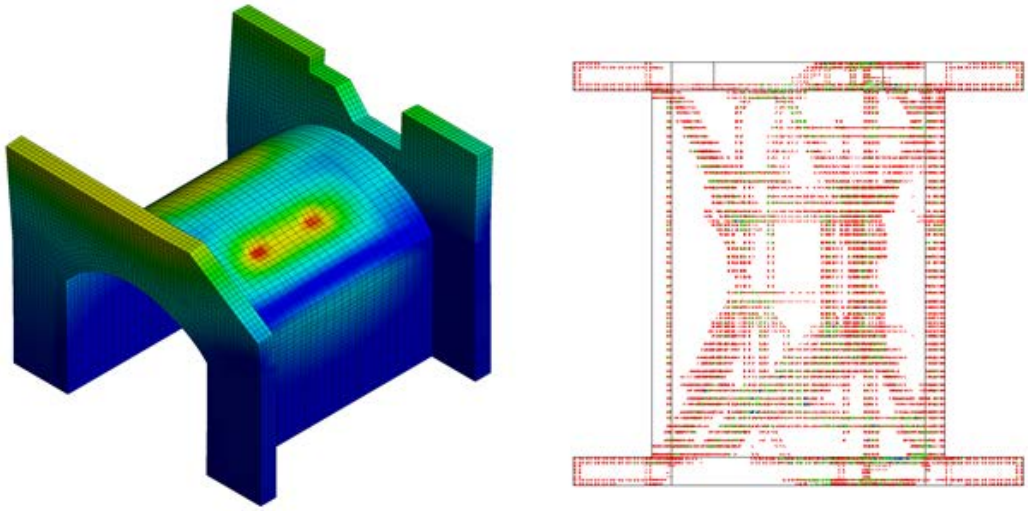

Figure 19 Scaled deflected shape and crack pattern at 167 tonnes for Greenfield Bridge

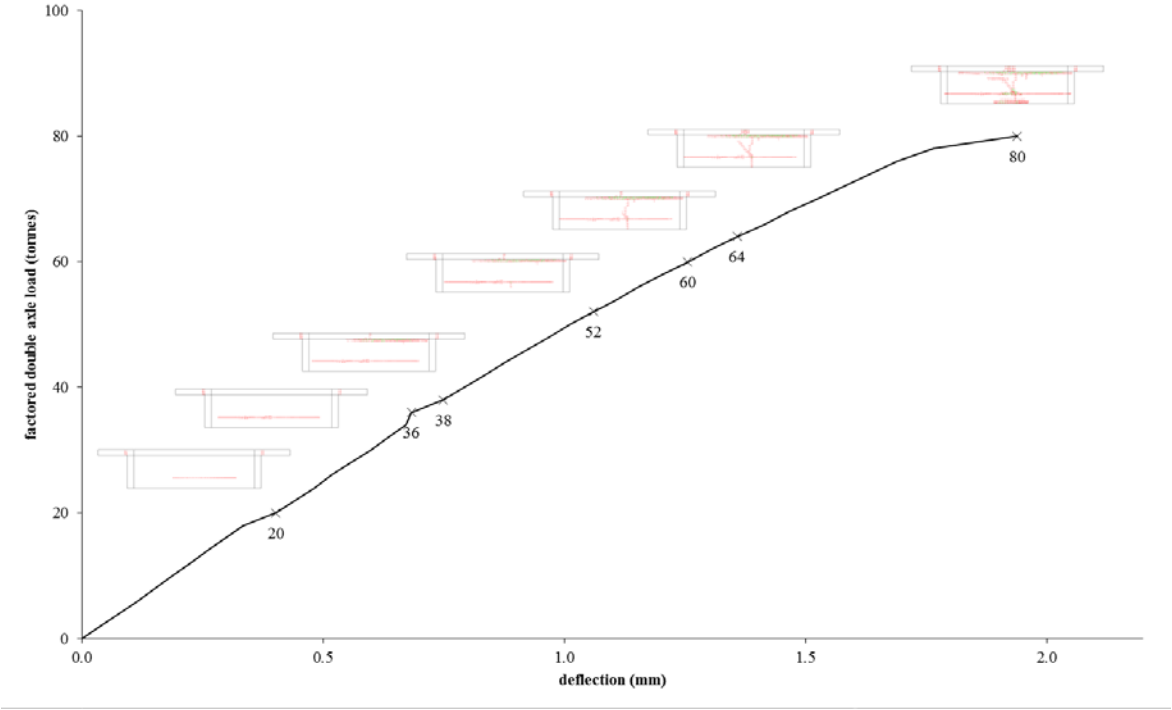

Figure 20 Load deflection response at crown centre for ultimate capacity prediction for O'Connell's Bridge

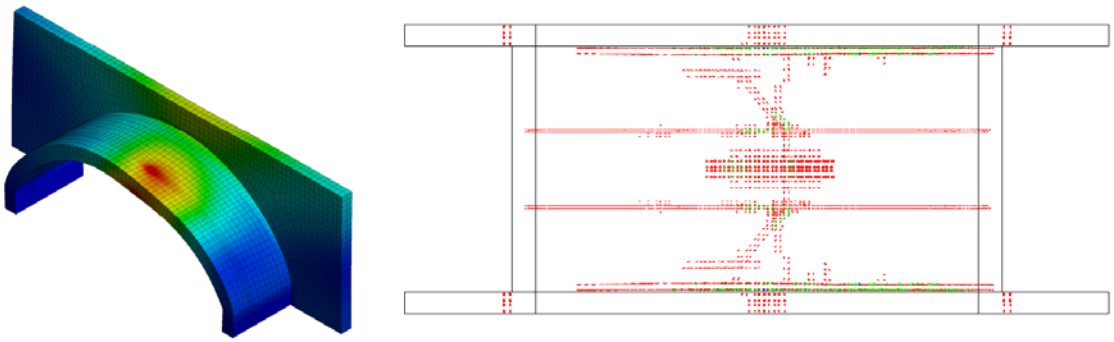

Figure 21 Scaled deflected shape and crack pattern at 80 tonnes for O'Connell's Bridge

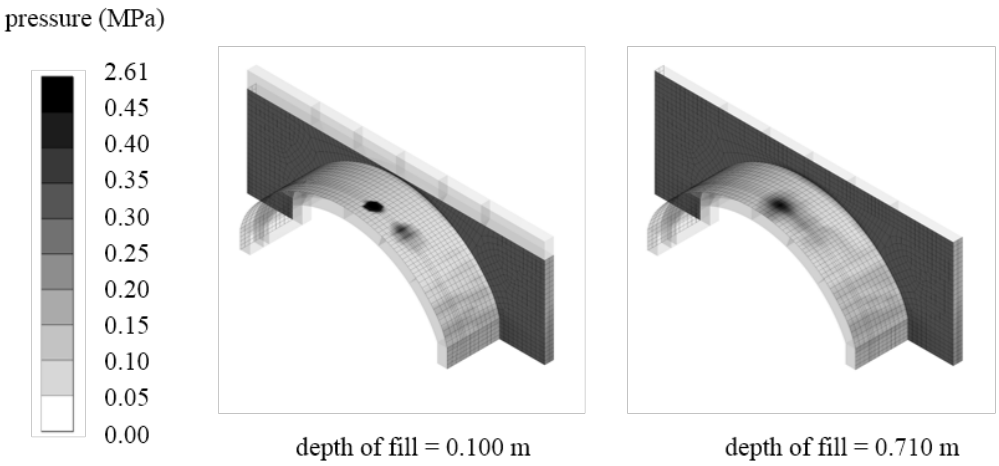

Figure 22 Contact pressure at 80 tonnes for O'Connell's Bridge with 0.100 m depth of fill (left) and 0.710 m depth of fill (right)

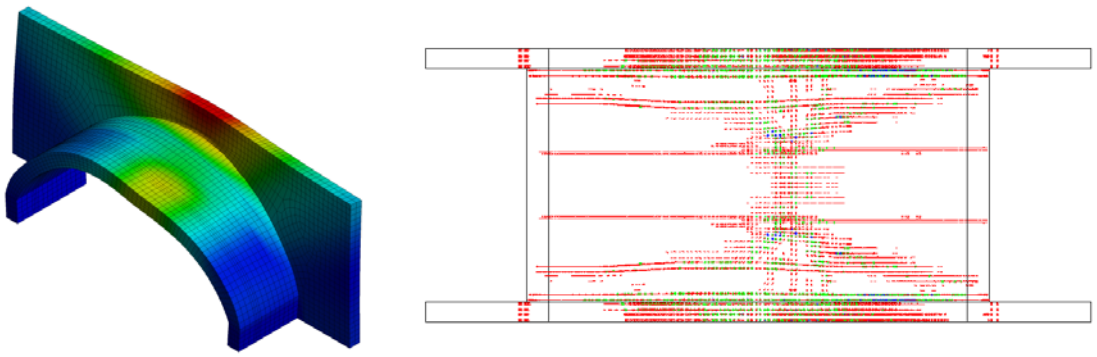

Figure 23 Scaled deflected shape and crack pattern at 124 tonnes for 0.710 m depth of fill for O'Connell's Bridge.

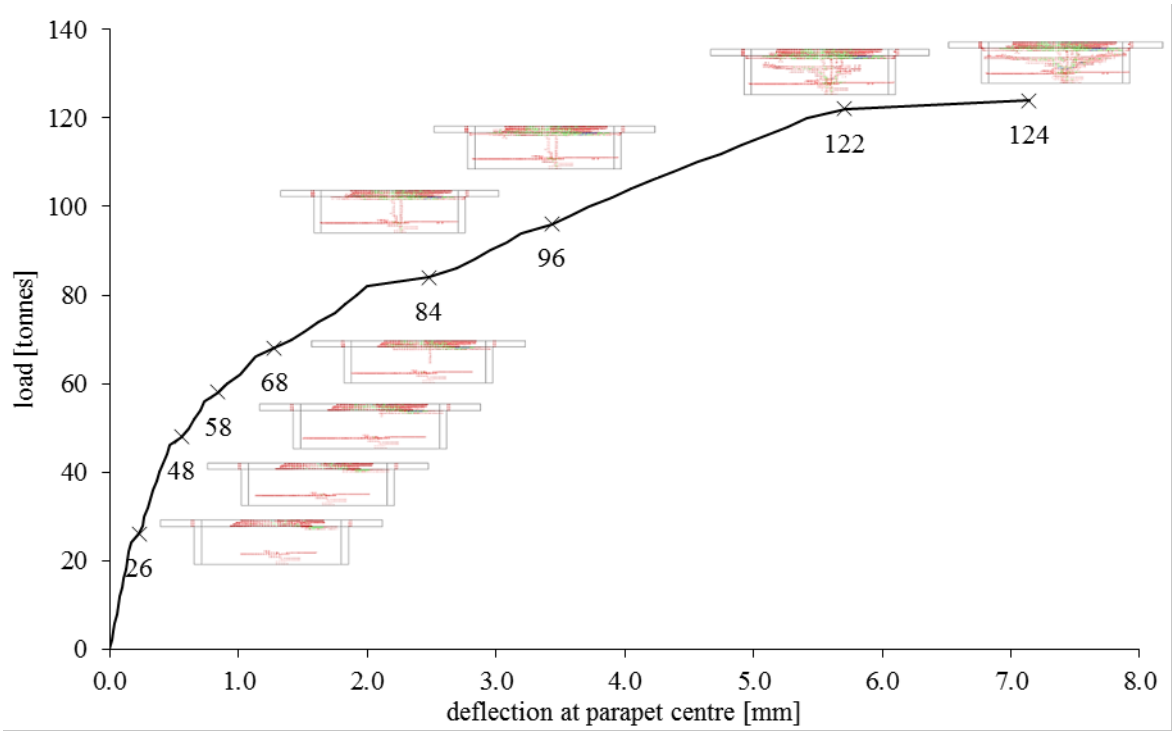

Figure 24 Load deflection response at parapet centre for 0.710 m depth of fill for O'Connell's Bridge